Elastocaloric determination of the phase diagram of Sr_2RuO_4

https://doi.org/10.1038/s41586-022-04820-z

Received: 6 December 2021

Accepted: 28 April 2022

Published online: 13 July 2022

Open access

Check for updates

You-Sheng Li[1], Markus Garst[2,3], Jörg Schmalian[3,4], Sayak Ghosh[5], Naoki Kikugawa[6], Dmitry A. Sokolov[1], Clifford W. Hicks[1,7], Fabian Jerzembeck[1], Matthias S. Ikeda[8,9,10], Zhenhai Hu[1], B. J. Ramshaw[5], Andreas W. Rost[11,12], Michael Nicklas[1]✉ & Andrew P. Mackenzie[1,11]✉

One of the main developments in unconventional superconductivity in the past two decades has been the discovery that most unconventional superconductors form phase diagrams that also contain other strongly correlated states. Many systems of interest are therefore close to more than one instability, and tuning between the resultant ordered phases is the subject of intense research[1]. In recent years, uniaxial pressure applied using piezoelectric-based devices has been shown to be a particularly versatile new method of tuning[2,3], leading to experiments that have advanced our understanding of the fascinating unconventional superconductor Sr_2RuO_4 (refs. [4–9]). Here we map out its phase diagram using high-precision measurements of the elastocaloric effect in what we believe to be the first such study including both the normal and the superconducting states. We observe a strong entropy quench on entering the superconducting state, in excellent agreement with a model calculation for pairing at the Van Hove point, and obtain a quantitative estimate of the entropy change associated with entry to a magnetic state that is observed in proximity to the superconductivity. The phase diagram is intriguing both for its similarity to those seen in other families of unconventional superconductors and for extra features unique, so far, to Sr_2RuO_4.

To establish the phase diagram of an unconventional superconductor, it is necessary to have both an effective means of tuning it and methods to investigate the resultant changes to its physical properties. In most of the systems studied so far, tuning methods such as chemical composition, magnetic field, electric field, hydrostatic and epitaxial pressure have been used. Each has its advantages and drawbacks, which ultimately determine the methods used to study the resultant phases and their interplay. An ideal method of study is one that has sensitivity to several phases simultaneously, and in particular to their boundaries. In magnetically tuned systems, the magnetocaloric effect has proved to be of particular utility. Under adiabatic conditions, the rate of change of the sample temperature with applied magnetic field H provides direct information on the heat capacity C_H and entropy S, through the well-known relationship

$$\left.\frac{\Delta T}{\Delta H}\right|_S \cong -\frac{T}{C_H}\left.\frac{\partial S}{\partial H}\right|_T, \quad (1)$$

which has been used to good effect to establish the H–T phase diagrams of, for example, URu_2Si_2 (ref. [10]) and $Sr_3Ru_2O_7$ (ref. [11]). As a tuning parameter, magnetic field brings advantages in terms of directionality and the ability to change symmetry, but also has the clear disadvantage that sufficiently high fields usually destroy, rather than promote, superconductivity. Uniaxial pressure brings the same advantage in terms of 'selective symmetry breaking' and does not automatically compete with superconductivity. In systems with a strong elastic response, the elastocaloric effect is a direct analogue of the magnetocaloric effect:

$$\left.\frac{\Delta T}{\Delta \varepsilon}\right|_S \cong -\frac{T}{C_\varepsilon}\left.\frac{\partial S}{\partial \varepsilon}\right|_T \quad (2)$$

in which C_ε is the specific heat at constant strain ε and $\left.\frac{\partial S}{\partial \varepsilon}\right|_T$ is the strain derivative of the entropy at constant temperature. In the special case of an isotropic volume strain $\Delta\varepsilon = \Delta V/V$, then $-\frac{1}{T}\frac{\Delta T}{\Delta \varepsilon}$ measures the famous Grüneisen parameter Γ originally introduced in 1908 (ref. [12]) and extensively studied in, for example, heavy fermion materials[13], but a generalized version of the Grüneisen parameter can also be defined for any combination of strain tensor components. If the relevant strain tunes the material through a quantum phase transition, the appropriate generalized Grüneisen parameter is an excellent tool with which to classify that transition[14,15].

[1]Max Planck Institute for Chemical Physics of Solids, Dresden, Germany. [2]Institut für Theoretische Festkörperphysik, Karlsruher Institut für Technologie, Karlsruhe, Germany. [3]Institut für QuantenMaterialien und Technologien, Karlsruher Institut für Technologie, Karlsruhe, Germany. [4]Institut für Theorie der Kondensierten Materie, Karlsruher Institut für Technologie, Karlsruhe, Germany. [5]Laboratory of Atomic and Solid State Physics, Cornell University, Ithaca, NY, USA. [6]National Institute for Materials Science, Tsukuba, Japan. [7]School of Physics and Astronomy, University of Birmingham, Birmingham, UK. [8]Geballe Laboratory for Advanced Materials, Stanford University, Stanford, CA, USA. [9]Department of Applied Physics, Stanford University, Stanford, CA, USA. [10]Stanford Institute for Materials and Energy Sciences, SLAC National Accelerator Laboratory, Menlo Park, CA, USA. [11]Scottish Universities Physics Alliance, School of Physics and Astronomy, University of St Andrews, St Andrews, UK. [12]Max Planck Institute for Solid State Research, Stuttgart, Germany. ✉e-mail: Michael.Nicklas@cpfs.mpg.de; Andy.Mackenzie@cpfs.mpg.de

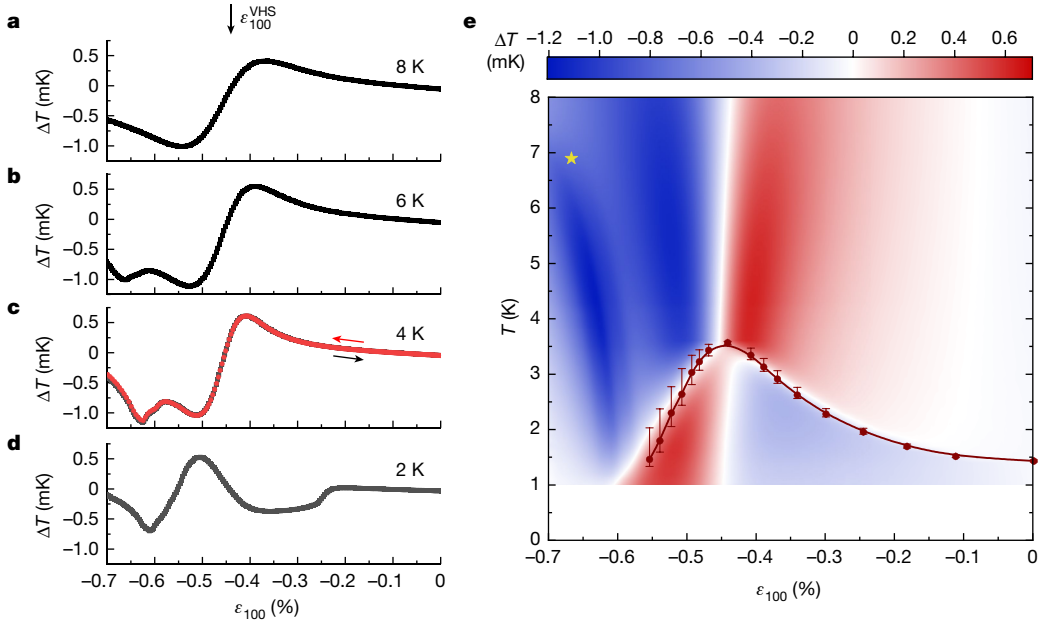

Fig. 1 | Response of the elastocaloric effect as a function of strain. a–**d**, The magnitude of the measured a.c. temperature against strain ε_{100} at different average sample temperatures, measured at 1,513 Hz and an excitation amplitude ε_{100}^{exc} between 2.9×10^{-6} and 3.5×10^{-6}. The strain at which the Van Hove singularity is traversed $\varepsilon_{100}^{VHS} = -0.44\%$ is indicated in panel **a**. The sign change of ΔT at ε_{100}^{VHS} corresponds to a maximum in the entropy. In panel **c**, data are shown for downsweeps and upsweeps at a rate of approximately 1% per hour. **e**, Colour map of the elastocaloric effect. Notice the pronounced entropy quench at T_c, at which the entropy changes from being maximal at ε_{100}^{VHS} for $T > T_c$ to forming a minimum at $T < T_c$. The solid red circles are the superconducting transition temperatures determined from measurements of the heat capacity[30]. The yellow star indicates the magnetic phase transition temperature obtained from μSR data[23], which agrees with the phase boundary identified by the dark blue contrast seen for ε_{100} between −0.6% and −0.7% in the elastocaloric effect. See Extended Data Figs. 1, 2 and 3 for further data.

Although used widely in association with materials with large elastic responses, to the extent that it has been proposed for cooling technologies[16,17], direct measurement of the elastocaloric effect has been much less widely used in the field of unconventional superconductivity or correlated electron physics, partly because the expected signal size is much smaller. Here we build on recent work using a.c. methods to perform high-resolution measurements of $\Delta T/\Delta\varepsilon$ in Fe-based superconductors[18–20] to study the elastocaloric effect in Sr_2RuO_4. As described in detail in Methods, we superimpose a small oscillatory component on the background steady strain and lock into the oscillatory component of the thermal response, which directly measures $\Delta T/\Delta\varepsilon$. We achieve the extremely high temperature measurement precision of approximately 2 μK $(\sqrt{Hz})^{-1}$ and use it to map out the phase diagram between 1 K and 8 K, for applied compressive strains along the [100] crystal axis of up to $\varepsilon_{100} = -0.7\%$, performing checks to ensure that we are close to the adiabatic limit for which Equation (2) applies. Our data allow us to determine Γ_{100}, the Grüneisen parameter for uniaxial stress applied along [100].

Sample raw data for isothermal strain sweeps at 8 K, 6 K, 4 K and 2 K are shown in Fig. 1a–d. Much can be learned from a qualitative inspection of the results. At 8 K, the data are seen to show the profile expected for a system in which a peak in entropy is studied under quasi-adiabatic conditions: the derivative changes sign at $\varepsilon_{100} \cong -0.44\%$, in line with previous estimates for the strain at which a Van Hove singularity is traversed at a so-called Lifshitz transition[5,8,21,22].

When the temperature has been lowered to 6 K, the signal at the Van Hove strain ε_{100}^{VHS} remains similar, but a pronounced extra dip is seen in the signal at around $\varepsilon_{100} \approx -0.6\%$. By 4 K, this dip has moved to slightly lower absolute strain and becomes stronger. The signal at 2 K looks similar to those at 4 K and 6 K at high strain but is very different in the region between −0.2% and −0.6% strain. Instead of a maximum of entropy at the Van Hove strain, there is now a minimum, along with a sharp step in the elastocaloric signal at $\varepsilon_{100} \cong -0.23\%$. Remarkably, this large change in the entropic properties is the result of the onset of superconductivity, as demonstrated by constructing the empirical phase diagram shown in Fig. 1e from interpolating the results of strain sweeps from 71 different temperatures, as described in Methods.

The high resolution of our experiments allows the straightforward identification of several key features from inspection of the raw data in Fig. 1e. First, above T_c, the strain at which the elastocaloric signal changes sign is nearly independent of temperature. This is the intuitive expectation for the elastocaloric signal of traversing a Van Hove singularity, which is expected to be independent of temperature in this temperature range because it is set by an underlying feature in the band structure and therefore determined by much higher energy scales. Within experimental uncertainty, it coincides with the maximum value of T_c and the strain at which the Van Hove singularity is observed to be crossed in photoemission experiments[8]. Second, the dispersion with strain of the dip seen for ε_{100} values of less than −0.6% (Fig. 1b–d) is reminiscent of that of a phase boundary. Third, the entropic signal of entering the superconducting state is extremely pronounced. The maximum in entropy as a function of strain at the Van Hove singularity is quenched, turning into a minimum below T_c. Away from the Van Hove point, the elastocaloric effect changes sign and almost reverses its magnitude near T_c. No signature of a second transition within the superconducting state[23] is resolved.

To frame a more in-depth analysis of our data, we turn to the behaviour of the relevant Grüneisen parameter $\Gamma_{100} \equiv -\frac{1}{T}\frac{\Delta T}{\Delta\varepsilon_{100}}$, converting the raw data to absolute units using the procedure described in Methods. In systems governed by a single energy scale, such as Fermi liquids, Γ is independent of temperature. As a result, Grüneisen scaling is expected with curves at all temperatures collapsing onto each other and deviations from this scaling indicating proximity to critical points or phase transitions[14,15]. We show this scaling in Fig. 2a for temperatures greater than the maximum superconducting transition temperature of 3.5 K. It is seen to be excellent for $-0.3\% < \varepsilon_{100} < 0$. Between −0.3% and −0.55%, the departure from scaling is of the kind qualitatively

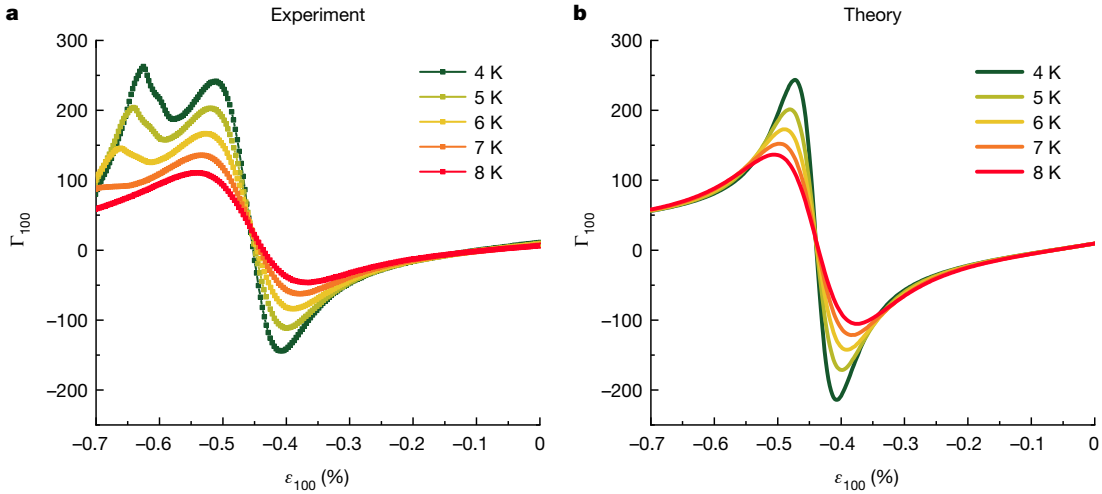

Fig. 2 | Grüneisen scaling. a, Experimental data converted to absolute units using a temperature-independent and strain-independent scale factor determined at 6 K using the procedure described in Methods. **b**, Theoretical calculations of Γ_{100} in the temperature range $T \geq 4$ K using a simple single-band, two-dimensional model. The sign change at $\varepsilon_{100} \approx -0.44\%$ can clearly be attributed to crossing the Van Hove point. A Grüneisen scaling collapse is observed for small strains $\varepsilon_{100} > -0.2\%$ in both panels. The extra peak at large strains for ε_{100} around −0.65% in panel **a** is attributed to magnetism that is not captured by the theory of panel **b**. A more realistic model including the full three-dimensional dispersion of Sr_2RuO_4 (Supplementary Information) gives essentially the same theoretical results.

expected for proximity to a quantum phase transition, in this case, the Lifshitz transition at $\varepsilon_{100} = -0.44\%$. For strains between −0.6% and −0.7%, the Grüneisen scaling is also poorly obeyed, supporting the hypothesis that the feature in this region (now a peak rather than a dip because of the sign convention of the Grüneisen parameter) marks a phase transition.

As a complement to the experimental data, we have calculated the expected behaviour of the Grüneisen parameter as a function of [100] strain using a two-dimensional tight-binding model for the relevant γ band derived from a combination of de Haas–van Alphen and angle-resolved photoemission experiments on unstrained Sr_2RuO_4 (ref. [24]). Full details are given in Methods and Supplementary Information.

The results are shown in Fig. 2b for the same range of temperatures as those in Fig. 2a. The qualitative agreement at strains $|\varepsilon_{100}| < |\varepsilon_{100}^{VHS}|$ is distinctive, especially given the simplicity of the model. The shape of the curves, the strain range over which the Grüneisen scaling is obeyed and even the zero crossing near zero strain (a consequence of the initial splitting of the zero-field Van Hove singularity owing to the Poisson effect) are all seen in both experiment and theory. By contrast, below 8 K, the behaviour for strains beyond ε_{100}^{VHS} is considerably different, emphasizing that the experimental data are picking up a phase transition not predicted by the tight-binding model. In isolation, the elastocaloric data give no microscopic information on the nature of the high-strain phase, but a point established in a recent muon spin relaxation measurement (marked by the yellow star in Fig. 1e) shows that it is magnetic, and probably a finite-Q state[23]. Establishing the boundary of this new phase is one of our key findings.

Next, we turn our attention to lower temperatures. In Fig. 3a, we show elastocaloric data at a range of temperatures between 3.7 K and 1 K. At 3.7 K, the sample is non-superconducting across the entire strain range, whereas at 1 K, it is superconducting for ε_{100} between −0.55% and 0. The behaviour at intermediate temperatures is prominent. After following

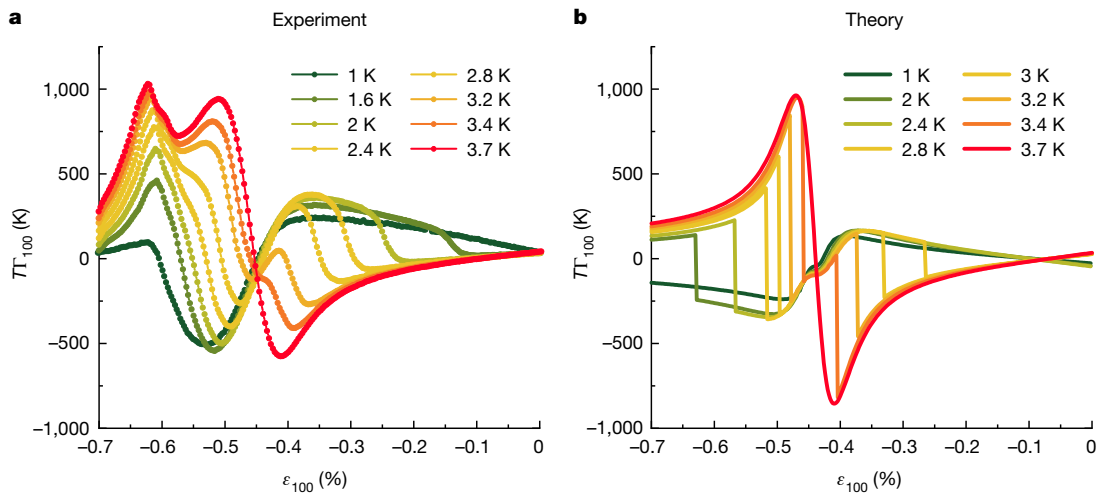

Fig. 3 | Elastocaloric effect. a, Experimental data converted to absolute units using the procedure described in the caption to Fig. 2. **b**, Theoretical calculations with a full gap at the Van Hove point of $T\Gamma_{100}$ in the temperature range $1\text{ K} \leq T \leq 3.7$ K using a simple single-band, two-dimensional model. The discontinuities in panel **b** identify the phase transition between the metallic and superconducting phases; these singularities are broadened in the experimental data in panel **a**. The extra peak at large strains for ε_{100} around −0.65% is attributed to magnetism.

the expected normal state behaviour at low strains, the signal abruptly reverses in sign owing to the entropy quench discussed above. On the high-strain side, the departure from the superconducting state becomes harder to distinguish and the signal increases rapidly in the region where superconducting and magnetic order approach each other.

Because there is, to our knowledge, no precedent in the literature of measurement of the elastocaloric signal on entry to the superconducting state, we constructed an illustrative model to frame the discussion of Fig. 3a. In Fig. 3b, we show the elastocaloric response obtained in a simple calculation: the density of states of the empirically constrained tight-binding model is combined with a strain-independent and k-independent pairing potential V to calculate the transition temperature of a hypothetical weak-coupled Bardeen–Cooper–Schrieffer superconductor that is fully gapped at the Van Hove points (see Supplementary Information). We do not claim that this model gives a full description of the superconductivity of Sr_2RuO_4 and certainly do not expect it to accurately predict $T_c(\varepsilon_{100})$ across the entire strain range, but it usefully highlights some of the key features of the experimental data. It demonstrates that the pronounced signal sign reversal that is so visually prominent in Fig. 3a for $-0.35\% < \varepsilon_{100} < -0.1\%$ on entry to the superconducting state can be understood within a very simple model of superconductivity. Consistent with the trend seen in the data, the large entropy at the Van Hove singularity arising from the enhanced density of states is strongly quenched on entering the superconducting state. By contrast, a second model calculation shows that our data cannot be reproduced by superconducting states with nodes at the Van Hove points (see Supplementary Information). Our data are therefore consistent only with superconducting order parameters that give a substantial gap in the vicinity of the Van Hove singularity. Nodal lines or points away from the Van Hove point are, of course, still possible.

Arguably as interesting as what the model successfully describes is what it does not. The theory–experiment comparison in Fig. 3 again highlights the notable qualitative difference in the experimental data on the low-stain and high-strain sides of ε_{100}^{VHS}. The models used to construct Figs. 2b and 3b do not include provision for a magnetic phase at high strain and predict a high degree of symmetry of both the normal state and the superconducting state signals around ε_{100}^{VHS}. The pronounced asymmetry in the data shows that the magnetic state exists and suggests that it affects the superconductivity.

It is possible to go further than qualitative statements and to extract the strain dependence of the entropy, using the analysis procedure described in Methods. Sample results at 4.5 K, 5.5 K, 6.5 K and 7.5 K are shown in Fig. 4. After peaking at the Van Hove strain, the entropy decreases as the strain is increased, with a more sudden decrease for $-0.61\% < \varepsilon_{100} < -0.68\%$, whose magnitude increases with decreasing temperature. At a first-order phase transition, the entropy shows a discontinuity, whereas we observe instead a rapid decrease of finite width. However, our experiment involves a small strain inhomogeneity, whose effects are clearly seen in Fig. 3 in the broadening of the signal as the superconducting state is entered. The strain width of the entropy decrease in Fig. 4 is similar, so the data probably indicate that the intrinsic decrease is discontinuous. The raw elastocaloric data highlight the qualitative difference between the signature of a peaking entropy (seen at ε_{100}^{VHS}) and the signature seen on entering the magnetic phase, which is a peak not in the entropy but in $-(\partial S/\partial\varepsilon)_T$. Overall, although we cannot be absolutely certain, we believe that our data support a first-order transition into the magnetic phase. Taking the peak in Γ_{100} as the transition point identifies it with the dark blue ridge in Fig. 1e. We can also quantify the change of entropy. The decrease in S/T at 4.5 K is approximately 3 mJ mol^{-1} K^{-2}, 8% of the electronic entropy of the unstrained material and more than 10% of the extrapolated background value at $\varepsilon_{100} = -0.63\%$. The absolute value is similar to that seen on entry to the low-temperature phase in $Sr_3Ru_2O_7$ (ref. [11]) but the sign is opposite. In Sr_2RuO_4, the entropy is lower in the magnetic phase than in the adjacent metal, in line with conventional expectation for a Fermi surface gapping transition.

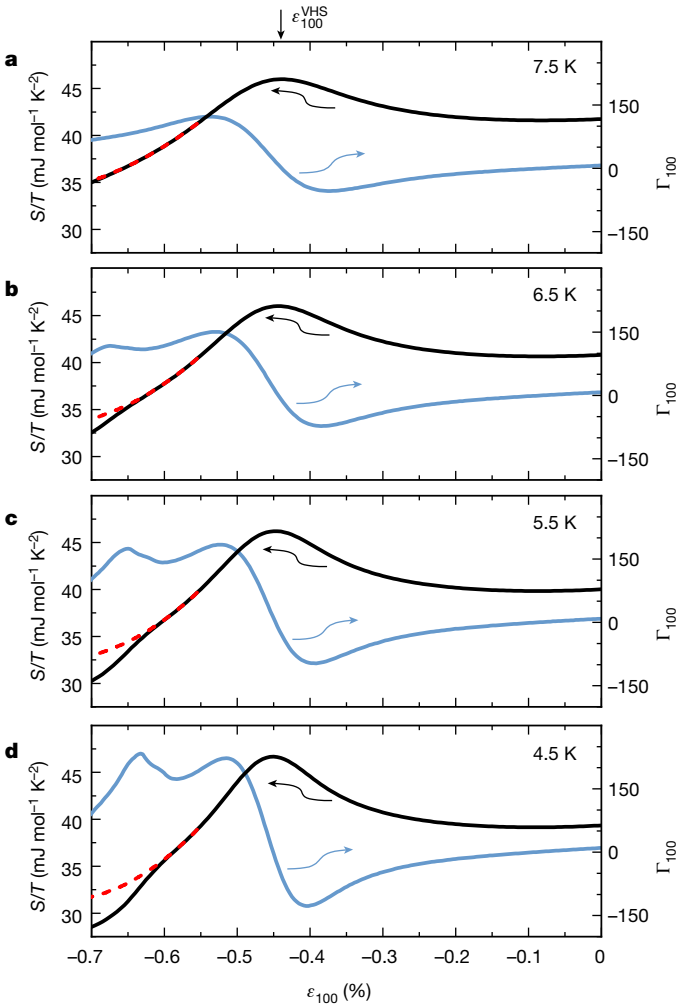

Fig. 4 | Strain dependence of the entropy. a–d, Integrating the Γ_{100} data using the iterative procedure described in Methods yields the strain-dependent entropy, plotted as S/T (black line) and directly compared with the measured Γ_{100} (blue line). The peak in Γ_{100} and corresponding rapid decrease of S/T indicates the magnetic transition at 4.5 K, 5.5 K and 6.5 K (**b–d**), whereas no decrease is visible at 7.5 K (**a**). The dotted red lines in the entropy traces are extrapolations of the background S/T from −0.55% to a lower cut-off consistent with the varying onset of the magnetic transition (−0.58%, −0.59%, −0.60% and −0.61% for 4.5 K, 5.5 K, 6.5 K and 7.5 K, respectively).

Independent of microscopic detail, the phase diagram determined by our measurements shows a strong and previously unappreciated experimental similarity between the tuned phase diagram of Sr_2RuO_4 and those of many cuprate, pnictide, organic and heavy fermion superconductors[25–28], in which superconductivity appears in the vicinity of a magnetic phase that is driven towards zero temperature by an external tuning parameter. This is especially timely given the recent evidence for an even-parity order parameter in Sr_2RuO_4 (ref. [9]), in common with those thought to exist in most of the above-mentioned materials. Our experiments also highlight the utility of the a.c. elastocaloric effect in the general study of unconventional superconductivity and correlated electron physics. As we have shown, the elastocaloric effect enables rapid and comprehensive phase diagram mapping and provides high-resolution datasets against which the quantitative predictions of theory can be tested. In the uniaxial pressure apparatus that we have developed[3,29], its combination with other experiments should be fairly straightforward, offering simultaneous access to spectroscopic and thermodynamic information from the same sample.

Online content

Any methods, additional references, Nature Research reporting summaries, source data, extended data, supplementary information, acknowledgements, peer review information; details of author contributions and competing interests; and statements of data and code availability are available at https://doi.org/10.1038/s41586-022-04820-z.

1. Fradkin, E., Kivelson, S. A. & Tranquada, J. M. *Colloquium*: Theory of intertwined orders in high temperature superconductors. *Rev. Mod. Phys.* **87**, 457–482 (2015).
2. Chu, J.-H. et al. In-plane resistivity anisotropy in an underdoped iron arsenide superconductor. *Science* **329**, 824–826 (2010).
3. Hicks, C. W., Barber, M. E., Edkins, S. D., Brodsky, D. O. & Mackenzie, A. P. Piezoelectric-based apparatus for strain tuning. *Rev. Sci. Instrum.* **85**, 65003 (2014).
4. Hicks, C. W. et al. Strong increase of T_c of Sr_2RuO_4 under both tensile and compressive strain. *Science* **344**, 283–285 (2014).
5. Steppke, A. et al. Strong peak in T_c of Sr_2RuO_4 under uniaxial pressure. *Science* **355**, eaaf9398 (2017).
6. Mackenzie, A. P., Scaffidi, T., Hicks, C. W. & Maeno, Y. Even odder after twenty-three years: the superconducting order parameter puzzle of Sr_2RuO_4. *npj Quantum Mater.* **2**, 40 (2017).
7. Barber, M. E., Gibbs, A. S., Maeno, Y., Mackenzie, A. P. & Hicks, C. W. Resistivity in the vicinity of a van Hove singularity: Sr_2RuO_4 under uniaxial pressure. *Phys. Rev. Lett.* **120**, 076602 (2018).
8. Sunko, V. et al. Direct observation of a uniaxial stress-driven Lifshitz transition in Sr_2RuO_4. *npj Quantum Mater.* **4**, 46 (2019).
9. Pustogow, A. et al. Constraints on the superconducting order parameter in Sr_2RuO_4 from oxygen-17 nuclear magnetic resonance. *Nature* **574**, 72–75 (2019).
10. Jaime, M., Kim, K. H., Jorge, G., McCall, S. & Mydosh, J. A. High magnetic field studies of the hidden order transition in URu_2Si_2. *Phys. Rev. Lett.* **89**, 287201 (2002).
11. Rost, A. W., Perry, R. S., Mercure, J.-F., Mackenzie, A. P. & Grigera, S. A. Entropy landscape of phase formation associated with quantum criticality in $Sr_3Ru_2O_7$. *Science* **325**, 1360–1363 (2009).
12. Grüneisen, E. Zusammenhang zwischen Kompressibilität, thermischer Ausdehnung, Atomvolumen und Atomwärme der Metalle. *Ann. Phys.* **331**, 393–402 (1908).
13. Gegenwart, P. Grüneisen parameter studies on heavy fermion quantum criticality. *Rep. Prog. Phys.* **79**, 114502 (2016).
14. Zhu, L., Garst, M., Rosch, A. & Si, Q. Universally diverging Grüneisen parameter and the magnetocaloric effect close to quantum critical points. *Phys. Rev. Lett.* **91**, 066404 (2003).
15. Garst, M. & Rosch, A. Sign change of the Grüneisen parameter and magnetocaloric effect near quantum critical points. *Phys. Rev. B* **72**, 205129 (2005).
16. Mañosa, L. & Planes, A. Materials with giant mechanocaloric effects: cooling by strength. *Adv. Mater.* **29**, 1603607 (2017).
17. Squillante, L., Mello, I. F., Seridonio, A. & de Souza, M. Giant caloric effects close to *any* critical end point. *Mater. Res. Bull.* **142**, 111413 (2021).
18. Ikeda, M. S. et al. AC elastocaloric effect as a probe for thermodynamic signatures of continuous phase transitions. *Rev. Sci. Instrum.* **90**, 083902 (2019).
19. Straquadine, J. A. W., Ikeda, M. S. & Fisher, I. R. Frequency-dependent sensitivity of AC elastocaloric effect measurements explored through analytical and numerical models. *Rev. Sci. Instrum.* **91**, 083905 (2020).
20. Ikeda, M. S. et al. Elastocaloric signature of nematic fluctuations. *Proc. Natl Acad. Sci. USA* **118**, e2105911118 (2021).
21. Barber, M. E. et al. Role of correlations in determining the van Hove strain in Sr_2RuO_4. *Phys. Rev. B* **100**, 245139 (2019).
22. Luo, Y. et al. Normal state ^{17}O NMR studies of Sr_2RuO_4 under uniaxial stress. *Phys. Rev. X* **9**, 021044 (2019).
23. Grinenko, V. et al. Split superconducting and time-reversal symmetry-breaking transitions in Sr_2RuO_4 under stress. *Nat. Phys.* **17**, 748–754 (2021).
24. Bergemann, C., Mackenzie, A. P., Julian, S. R., Forsythe, D. & Ohmichi, E. Quasi-two-dimensional Fermi liquid properties of the unconventional superconductor Sr_2RuO_4. *Adv. Phys.* **52**, 639–725 (2003).
25. Knebel, G. et al. Antiferromagnetism and superconductivity in $CeRhIn_5$. *J. Phys. Soc. Jpn* **80**, SA001 (2011).
26. Nandi, S. et al. Anomalous suppression of the orthorhombic lattice distortion in superconducting $Ba(Fe_{1-x}Co_x)_2As_2$ single crystals. *Phys. Rev. Lett.* **104**, 057006 (2010).
27. Sachdev, S. in *Modern Theories of Many-Particle Systems in Condensed Matter Physics. Lecture Notes in Physics* Vol. 843 (eds Cabra, D., Honecker, A. & Pujol, P.) 1–51 (Springer, 2012).
28. Doiron-Leyraud, N. et al. Correlation between linear resistivity and T_c in the Bechgaard salts and the pnictide superconductor $Ba(Fe_{1-x}Co_x)_2As_2$. *Phys. Rev. B* **80**, 214531 (2009).
29. Barber, M. E., Steppke, A., Mackenzie, A. P. & Hicks, C. W. Piezoelectric-based uniaxial pressure cell with integrated force and displacement sensors. *Rev. Sci. Instrum.* **90**, 23904 (2019).
30. Li, Y.-S. et al. High-sensitivity heat-capacity measurements on Sr_2RuO_4 under uniaxial pressure. *Proc. Natl Acad. Sci. USA* **118**, e2020492118 (2021).

Methods

Sample preparation and experimental setup

High-quality single crystals of Sr_2RuO_4 were grown by a floating-zone method[31]. Special care was taken to select the sample from a region with the highest T_c and the absence of a signal from '3-K phase' inclusions, indicating the highest quality Sr_2RuO_4. The sample was aligned along the [100] crystallographic direction by Laue X-ray diffraction and needles were wire sawed and polished using diamond-impregnated sheets with different grain sizes down to 1 μm to obtain parallel surfaces and to reduce the surface roughness. A home-made Au/AuFe (0.07%) thermocouple (25 μm wire diameter) served as a thermometer to measure the a.c. temperature changes. It was independently calibrated using procedures outlined in ref. [30] and attached to the centre of the sample using silver epoxy (Dupont 6838), soldered to twisted copper wires that were thermally anchored on the thermometry stage. The assembly was subsequently glued in the jaws of a uniaxial pressure cell using Stycast 2850FT epoxy with Catalyst 23LV. Special care was taken to minimize the tilt of the sample and to ensure a force transmission along the long axis of needle. The sample temperature was measured using calibrated resistive low-temperature sensors. The present experimental setup with the same sample was used in a previous heat capacity study[30,32]. Schematic diagrams of the experimental setup are shown in Extended Data Fig. 4a,b.

Measurement of the elastocaloric effect

The elastocaloric effect was measured by an a.c. modulation method[18]. The uniaxial pressure apparatus was mounted to the cold plate of a dilution refrigerator (Oxford Instruments). To achieve the large strains needed to tune Sr_2RuO_4 in the desired range, large d.c. voltages had to be applied on both inner and outer piezoactuators of the uniaxial pressure apparatus. A home-made high-voltage amplifier was used to drive the outer piezoactuators. The a.c.-modulated strain was achieved by superimposing an a.c. voltage on top of a d.c. voltage on the inner piezoactuator. To amplify the coupled a.c. and d.c. voltages, a commercial high-voltage amplifier was used (TEGAM 2350, bandwidth d.c. to 2 MHz). The extremely low noise level of 20 pV $(\sqrt{Hz})^{-1}$ on the thermocouple readout, corresponding to 5.1 μK $(\sqrt{Hz})^{-1}$, 2.1 μK $(\sqrt{Hz})^{-1}$ and 1.7 μK $(\sqrt{Hz})^{-1}$ at 1 K, 4 K and 8 K, respectively, was obtained by the use of a high-frequency low-temperature transformer (CMR-Direct), operating at a gain of 300, mounted on the 1-K pot of the dilution refrigerator. Its output was read by an EG&G 7265 lock-in amplifier. We show the configuration of the electronic setup for the ultra-low-noise measurement of the temperature oscillations in Extended Data Fig. 4c.

Determination of the applied uniaxial strain in the sample

Strain is the change of the length of a sample $\Delta l = l - l_0$ divided by its length l_0. The strain apparatus used in this study has a capacitor to measure the displacement Δd obtained by applying a voltage to the piezoelectric actuators (PEAs). However, the measured Δd is not the change in the sample length. Δl can be obtained by the change of the capacitor displacement Δd times a transfer efficiency e, which is defined by the properties of Stycast layers between the sample and the jaws of the strain apparatus[3]. Therefore, we find for the strain in the sample:

$$\varepsilon = \frac{\Delta l}{l} = \frac{e \times \Delta d}{l_0}. \tag{3}$$

In the case of Sr_2RuO_4 in the current setup, a transfer efficiency $e = 0.78$ could be estimated on the basis of the known position of the maximum in T_c for an applied stress along [100] at 0.7 GPa (ref. [29]) and the Young's modulus $E_Y = 160$ GPa at 4 K (ref. [33]).

To obtain the large strains needed to investigate the phase diagram of Sr_2RuO_4, the inner and outer PEAs of the strain apparatus are used. To measure the elastocaloric effect, a further small a.c. voltage is imposed on the d.c. voltage applied on the inner PEA. The oscillation amplitude d_{exc} can be measured using the capacitor mounted in parallel to the sample and the strain amplitude is then obtained following Equation (3):

$$\Delta\varepsilon = \frac{e \times d_{exc}}{l_0}. \tag{4}$$

In our case, the displacement amplitude d_{exc} is between 5 nm and 10 nm, in comparison with a sample length of approximately 2 mm. Strain is a tensor quantity, so a formal definition of ε_{100} as used in the main text is $\varepsilon_{100} = \vec{e}_{100} \bullet \hat{\varepsilon} \bullet \vec{e}_{100}$, in which $\vec{e}_{100} = (1,0,0)$.

Adiabaticity of the measurement

Curves of ΔT against frequency at 0.5% compression are shown in Extended Data Fig. 5 on a double-logarithmic representation. One can easily identify the lower cut-off frequency, between 100 Hz and 300 Hz. In the high-frequency range, this is not possible because the data start to scatter strongly above a few kilohertz before the upper cut-off frequency is reached. The enhanced noise is related to vibrations of thermocouple wires. Between 1 K and 8 K, we do not observe a notable change in the upper frequency boundary. This implies that the upper cut-off frequency is at least larger than 10 kHz. Here we chose a measuring frequency $f = 1{,}513$ Hz, which corresponds to ΔT on the plateau of the frequency response. The phase response is around zero for all temperatures between 1 K and 8 K at $f = 1{,}513$ Hz.

Estimation of the elastocaloric signal size

In principle, the absolute value of the elastocaloric effect can be obtained directly. However, owing to the smallness of the signal and uncertainties arising from sample configuration and material properties, it is more reliable to calibrate the elastocaloric effect $\Delta T_{ad}/\Delta\varepsilon$, as described in the following.

The elastocaloric effect can be described as an adiabatic temperature change ΔT_{ad} as a function of strain ε:

$$\frac{\Delta T_{ad}}{\Delta\varepsilon} \cong -\frac{T}{C_{\varepsilon,\sigma_y,\sigma_z}}\left(\frac{\partial S}{\partial\varepsilon}\right)_{T,\sigma_y,\sigma_z} \tag{5}$$

Here $C_{\varepsilon,\sigma_y,\sigma_z}$ is the heat capacity at constant strain and S is the entropy. The relevant elastocaloric Grüneisen parameter Γ in our experiment is related to entropy through

$$\Gamma = \frac{(\partial S/\partial\varepsilon)_{T,\sigma_y,\sigma_z}}{C_{\varepsilon,\sigma_y,\sigma_z}} = \frac{(\partial S/\partial\varepsilon)_{T,\sigma_y,\sigma_z}}{T\,(\partial S/\partial T)_{\varepsilon,\sigma_y,\sigma_z}} = -\frac{1}{T}\left(\frac{\partial T}{\partial\varepsilon}\right)_{S,\sigma_y,\sigma_z} \tag{6}$$

Please note that, throughout this section, ε refers to ε_{xx}. At very low strains on the order of −0.1% at temperatures above the superconducting transition, one can treat the system as being a Fermi liquid whose parameters are a function of strain. In this case, the specific heat to the second order in strain is given by

$$C(\varepsilon, T) = \gamma\,(1 + \varepsilon\gamma_1/\gamma + \varepsilon^2\gamma_2/\gamma)\,T + \beta T^3 \tag{7}$$

Here we further assumed that the phonon heat capacity in our case has a negligible strain dependence. This is justified by both the small strain limit considered and the fact that the phonon contribution is much smaller than the electronic heat capacity at the relevant temperatures in the first place. It directly follows that entropy S is given by

$$S(\varepsilon, T) = \int_0^T \frac{C(\varepsilon, T)}{T}\mathrm{d}T = (\gamma + \gamma_1\varepsilon + \gamma_2\varepsilon^2)\,T + \frac{1}{3}\beta T^3 \tag{8}$$

In this limit, the elastocaloric Grüneisen parameter Γ can be expressed as

$$\Gamma = \frac{(\gamma_1 + 2\gamma_2\varepsilon)\,T}{(\gamma + \gamma_1\varepsilon + \gamma_2\varepsilon^2)\,T + \beta T^3} \tag{9}$$

and

$$(\partial S/\partial\varepsilon)_{T,\sigma_y,\sigma_z} = \quad (\gamma_1 + 2\gamma_2\varepsilon)\,T \tag{10}$$

Furthermore, one can consider the second derivative of entropy with respect to strain

$$\left(\frac{\partial^2}{\partial\varepsilon^2}S\right)_{T,\sigma_y,\sigma_z} = \left(\frac{\partial}{\partial\varepsilon}\left(\frac{\partial S}{\partial\varepsilon}\right)_{T,\sigma_y,\sigma_z}\right)_{T,\sigma_y,\sigma_z} = -\left(\frac{\partial}{\partial\varepsilon}\left(\frac{\partial\sigma_x}{\partial T}\right)_{\varepsilon,\sigma_y,\sigma_z}\right)_{T,\sigma_y,\sigma_z} \tag{11}$$

in which we made use of the appropriate Maxwell relationship in the last step. Given that in the range considered here thermodynamic variables are well behaved, it follows that

$$\left(\frac{\partial^2}{\partial\varepsilon^2}S\right)_{T,\sigma_y,\sigma_z} = -\left(\frac{\partial}{\partial T}\left(\frac{\partial\sigma_x}{\partial\varepsilon}\right)_{T,\sigma_y,\sigma_z}\right)_{\varepsilon,\sigma_y,\sigma_z} \tag{12}$$

in which stress ε and strain σ are related by means of the compliance matrix $\underline{\underline{\mathbf{s}}}$ through $\boldsymbol{\varepsilon} = \underline{\underline{\mathbf{s}}}\boldsymbol{\sigma}$. Hence

$$\left(\frac{\partial^2}{\partial\varepsilon^2}S\right)_{T,\sigma_y,\sigma_z} = -\left(\frac{\partial}{\partial T}s_{11}^{-1}\right)_{\varepsilon,\sigma_y,\sigma_z} \tag{13}$$

with s_{11} being the 11 entry of $\underline{\underline{\mathbf{s}}}$ and the inverse of the Young's modulus.

Combining Equations (10) and (13) therefore yields

$$2\gamma_2 T = -\left(\frac{\partial}{\partial T}s_{11}^{-1}\right)_{\varepsilon,\sigma_y,\sigma_z} \tag{14}$$

s_{11} determined from resonant ultrasound experiments using methods described in ref. [33] is shown in Extended Data Fig. 6a, together with a fit of the form

$$s_{11} = s_{11,0} + s_{11,2}T^2 \tag{15}$$

giving $s_{11,2} = 1.526 \times 10^{-7}\ \mathrm{GPa^{-1}\,K^{-2}}$ and $\gamma_2 = \frac{s_{11,2}}{s_{11}^2} \approx \frac{s_{11,2}}{s_{11,0}^2} = 0.0039\ \mathrm{GPa\,K^{-2}}$.

The elastocaloric Grüneisen parameter is therefore fully determined except for γ_1, permitting us to calibrate our measured data by means of an overall amplitude factor $\Gamma = a\Gamma^{\mathrm{meas}}$,

$$\Gamma^{\mathrm{meas}} = \frac{1}{a}\,\frac{(\gamma_1 + 2\gamma_2\varepsilon)\,T}{(\gamma + \gamma_1\varepsilon + \gamma_2\varepsilon^2)\,T + \beta T^3} \tag{16}$$

γ, β and $s_{11,2}$ are constrained by independent experiments, with a and γ_1 being the only independent parameters.

In Extended Data Fig. 6b, we show Γ^{meas} for temperatures between 5.5 K and 6.5 K and small strains for up to −0.1%, for which the above approximations are valid. The surface shown is a fit of the functional form of Equation (16). The fit gives $a = 2.90$ and $\gamma_1 = 6{,}797\ \mathrm{J\,m^{-3}\,K^{-1}}$.

Numerical calculation of the entropy

Here we describe the numerical scheme for the calculation of entropy shown in Fig. 4.

Our starting point is

$$\Gamma_\varepsilon = \frac{1}{C_{\varepsilon_{xx}}}\left(\frac{\partial S}{\partial\varepsilon_{xx}}\right)_T \tag{17}$$

Simple rearrangement gives

$$(\partial S/\partial\varepsilon_{xx})_T \quad = C_{\varepsilon_{xx}}\Gamma_\varepsilon \tag{18}$$

With the knowledge of the entropy at zero strain, $S(\varepsilon = 0, T)$, one can integrate this partial differential to give

$$S(\varepsilon, T) = \int_0^\varepsilon C_{\varepsilon_{xx}}(\varepsilon', T) \quad \Gamma_\varepsilon(\varepsilon', T)\,\mathrm{d}\varepsilon' + S(\varepsilon = 0, T) \tag{19}$$

$\Gamma_\varepsilon(\varepsilon, T)$ is known from the experiments, whereas $C_{\varepsilon_{xx}}(\varepsilon, T)$ is, at this stage, unknown. However, it is related to $S(\varepsilon, T)$ through

$$C_{\varepsilon_{xx}}(\varepsilon', T) = T\left(\frac{\partial S}{\partial T}\right)_{\varepsilon_{xx}} \tag{20}$$

We therefore use an iterative scheme with the following steps. First, set $C^{(0)}_{\varepsilon_{xx}}(\varepsilon_{xx}, T) = C(0, T)$. This is the zero-strain specific heat, known with very high accuracy for Sr_2RuO_4. Second, calculate $S^{(0)}(\varepsilon_{xx}, T)$ using Equation (19) and $C^{(0)}_{\varepsilon_{xx}}(\varepsilon_{xx}, T)$ for all available T. Third, calculate $C_{\varepsilon_{xx}}(\varepsilon_{xx}, T)$ by interpolating $S^{(0)}(\varepsilon_{xx}, T)$ as a function of T and evaluating Equation (20). Finally, calculate $S^{(1)}(\varepsilon_{xx}, T)$ using $C^{(1)}_{\varepsilon_{xx}}(\varepsilon_{xx}, T)$ and Equation (19), an iteration of the second step.

After a few iterations, no notable changes in $S^{(n)}(\varepsilon, T)$ are observed. This is not least due to the fact that, although $C_{\varepsilon_{xx}}$ does vary overall, these variations are at most a few tens of per cent, enabling an effective convergence of the above scheme. The data shown in the main text correspond to $S^{(2)}$.

Theoretical analysis

The theoretical analysis of the elastocaloric effect is on the basis of a quasiparticle description of Sr_2RuO_4. We use a strain-dependent quasiparticle dispersion $\varepsilon_{\mathbf{k}}(\epsilon_{\alpha\beta})$ and determine the electronic contribution to the entropy of the system from

$$S_{\mathrm{el}} = -\frac{2k_{\mathrm{B}}}{N}\ \sum_{\mathbf{k}}\ [f_{\mathbf{k}}\log f_{\mathbf{k}} + (1-f_{\mathbf{k}})\log(1-f_{\mathbf{k}})].$$

$f_{\mathbf{k}}$ is the Fermi distribution function with the above dispersion. The factor 2 refers to the electron spin and the sum goes over the momenta in the first Brillouin zone. The elastocaloric coefficient follows from the temperature and strain derivatives of the entropy. We use the following tight-binding parameterization for the γ-band of the system as determined from angle-resolved photoemission experiments[34]:

$$\varepsilon_{\mathbf{k}} = -2t_x\cos(k_x a_x) - 2t_y\cos(k_y a_y) - 4t'\cos(k_x a_x)\cos(k_y a_y) - \mu,$$

with $t_x = t_y = t_0 = 0.119$ eV, $t' = 0.392t_0$ and $\mu = 1.48t_0$. To describe the strain dependence of $\varepsilon_{\mathbf{k}}(\epsilon_{\alpha\beta})$, we assume a linear dependence of the hopping elements with respect to the interatomic distance. The proportionality factor is chosen to reproduce the strain value at which the Van Hove singularity is reached. In the superconducting state, we use the Bogoliubov quasiparticle dispersion $\varepsilon_{\mathbf{k}} \to \sqrt{\varepsilon_{\mathbf{k}}^2 + \Delta^2}$ with superconducting gap Δ. The strain dependence is dominated by the electronic spectrum near the Van Hove point. In our theory, we consider a pairing state that is fully gapped at the Van Hove momentum. The strain dependence of the superconducting gap amplitude and of the transition temperature follow from the solution of the gap equation at fixed pairing interaction. For details, see the Supplementary Information.

Data availability

The data that underpin the findings of this study are available at https://doi.org/10.17630/6a4a06c6-38d3-464f-88d1-df8d2dbf1e75.

31. Bobowski, J. S. et al. Improved single-crystal growth of Sr_2RuO_4. *Condens. Matter* **4**, 6 (2019).
32. Li, Y.-S., Borth, R., Hicks, C. W., Mackenzie, A. P. & Nicklas, M. Heat-capacity measurements under large uniaxial pressure using a piezo-driven device. *Rev. Sci. Instrum.* **91**, 103903 (2020).
33. Ghosh, S. et al. Thermodynamic evidence for a two-component superconducting order parameter in Sr_2RuO_4. *Nat. Phys.* **17**, 199–204 (2021).
34. Burganov, B. et al. Strain control of fermiology and many-body interactions in two-dimensional ruthenates. *Phys. Rev. Lett.* **116**, 197003 (2016).

Acknowledgements We are grateful to S. Kivelson for helpful discussions. This work was supported by the Max Planck Society and the Deutsche Forschungsgemeinschaft (DFG, German Research Foundation) – TRR 288-422213477 ELASTO-Q-MAT (projects A10 (C.W.H. and A.P.M.), A11 (M.G.) and B01 (J.S.)). S.G. and B.J.R. acknowledge funding from the U.S. Department of Energy, Office of Basic Energy Sciences under award number DESC0020143. This work made use of the Cornell Center for Materials Research (CCMR) Shared Facilities, which is supported through the NSF MRSEC programme (no. DMR-1719875) (S.G. and B.J.R.). N.K. acknowledges support from KAKENHI Grants-in-Aid for Scientific Research (grant nos. 17H06136, 18K04715 and 21H01033) and Core-to-Core Program (no. JPJSCCA20170002) from the Japan Society for the Promotion of Science (JSPS) and by a JST-Mirai Program (grant no. JPMJMI18A3). A.W.R. acknowledges support from the Engineering and Physical Sciences Research Council (grant numbers EP/P024564/1, EP/S005005/1 and EP/V049410/1). Research in Dresden benefits from the environment created by the DFG Excellence Cluster 'Correlations and Topology in Quantum Materials'.

Author contributions Y.-S.L. performed the experiments and analysed the data, with input from M.S.I., M.N., Z.H., A.W.R., C.W.H. and A.P.M.; M.G. and J.S. constructed the theoretical models; S.G. and B.J.R. conducted further resonant ultrasound experiments; A.W.R. and Z.H. designed and tested the entropy calculation and signal calibration protocols; N.K., D.A.S. and F.J. grew and characterized the crystals; C.W.H. developed the uniaxial pressure apparatus. A.P.M. conceived the project and wrote the paper, with input from all co-authors.

Funding Open access funding provided by Max Planck Society.

Competing interests The authors declare no competing financial interests.

Additional information

Supplementary information The online version contains supplementary material available at https://doi.org/10.1038/s41586-022-04820-z.

Correspondence and requests for materials should be addressed to Michael Nicklas or Andrew P. Mackenzie.

Peer review information *Nature* thanks Thierry Klein, Cedric Weber and the other, anonymous, reviewer(s) for their contribution to the peer review of this work.

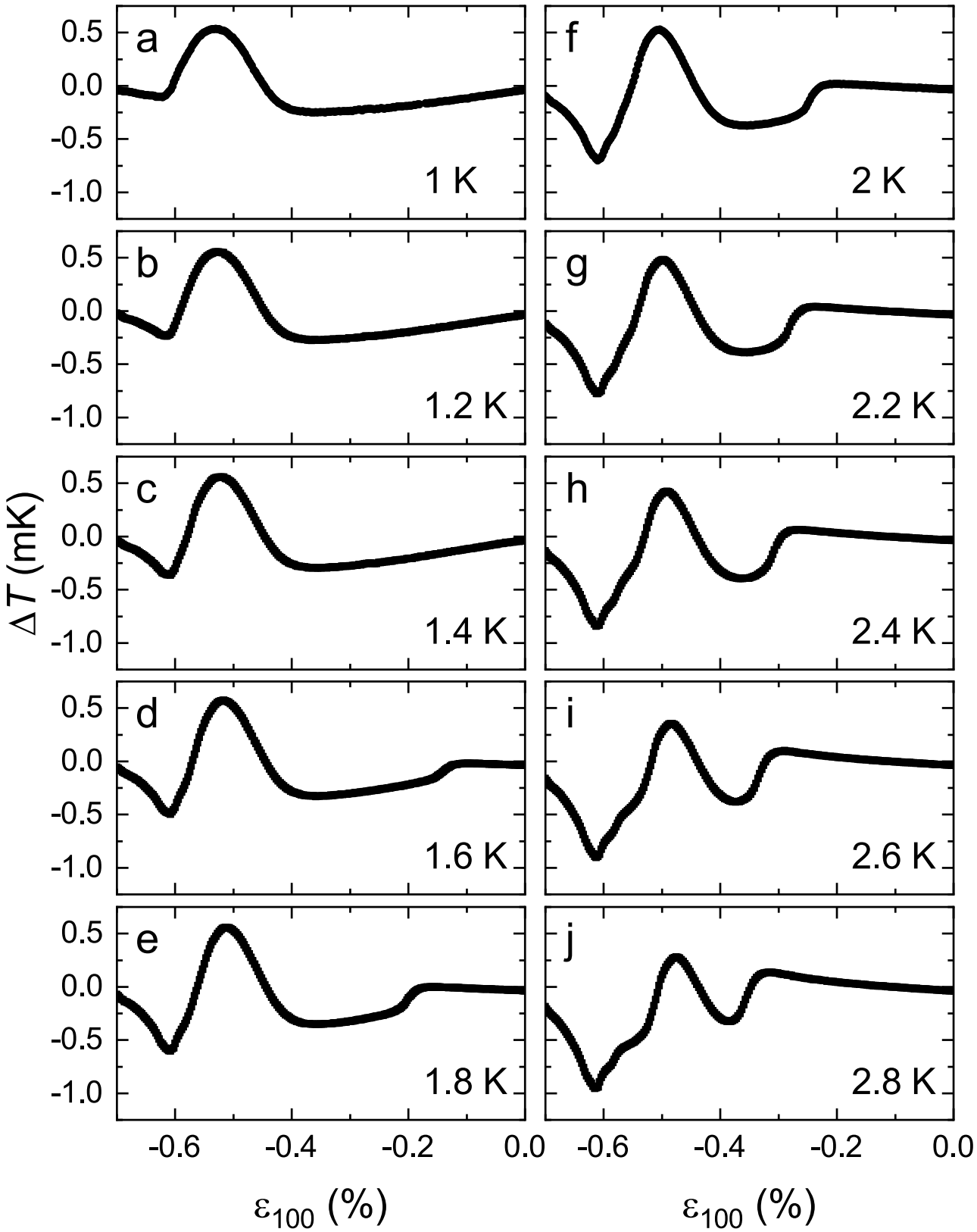

Extended Data Fig. 1 | Response of the elastocaloric effect as a function of strain (further data: low temperatures). $\Delta T(\varepsilon_{100})$ recorded at 1,513 Hz with an excitation amplitude ε_{100}^{exc} between 2.9×10^{-6} and 3.5×10^{-6} during strain sweeps at ten different temperatures from 1 K to 2.8 K.

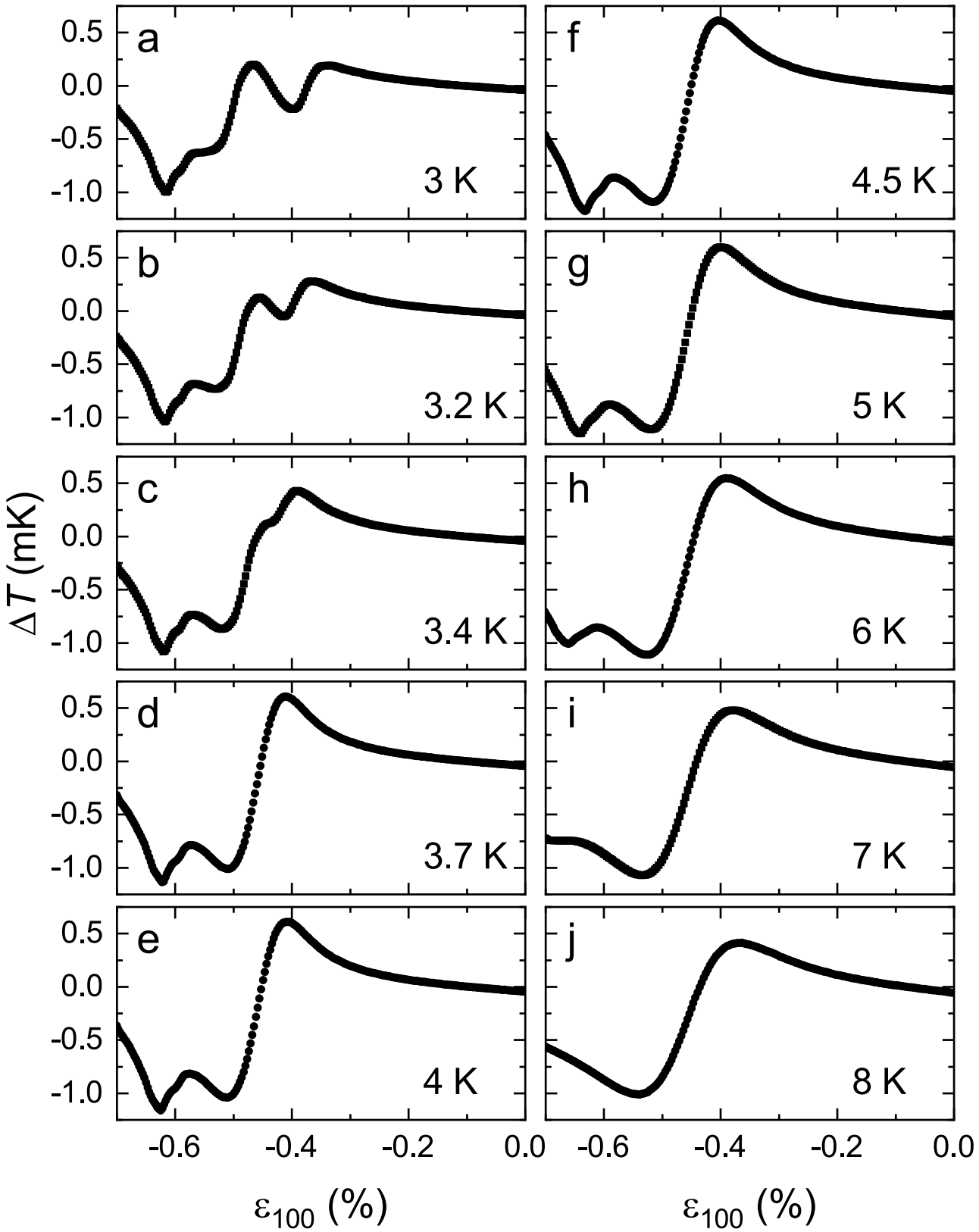

Extended Data Fig. 2 | Response of the elastocaloric effect as a function of strain (further data: high temperatures). $\Delta T(\varepsilon_{100})$ recorded at 1,513 Hz with an excitation amplitude ε_{100}^{exc} between 2.9×10^{-6} and 3.5×10^{-6} during strain sweeps at ten different temperatures from 3 K to 8 K.

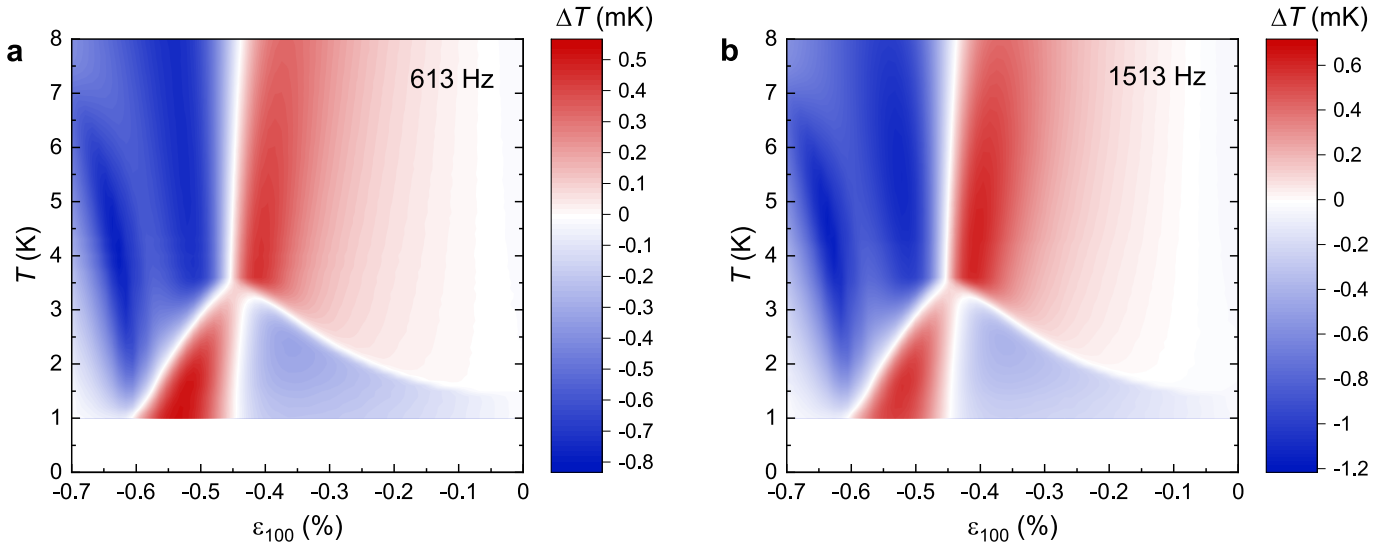

Extended Data Fig. 3 | Comparison of the colour maps of the elastocaloric effect taken at different frequencies. Data taken at 613 Hz (**a**) and at 1,513 Hz (**b**). The data were recorded with an excitation amplitude ε_{100}^{exc} between 2.9×10^{-6} and 3.5×10^{-6}.

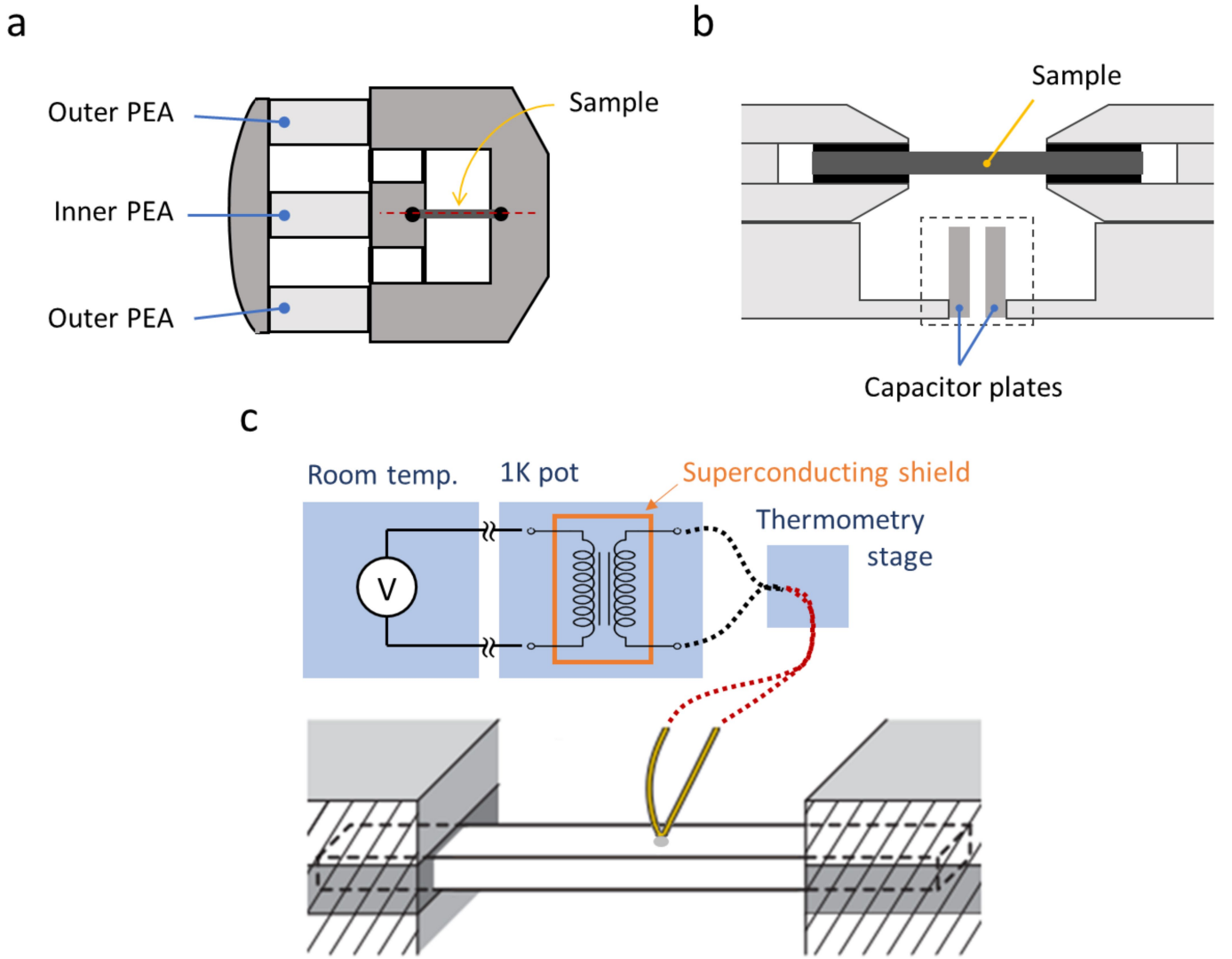

Extended Data Fig. 4 | Schematic diagrams of the experimental setup. **a**, A uniaxial strain cell with inner and outer piezoelectric actuators (PEAs). To vary the tuning strain on the sample, the outer PEAs were driven between −350 V and 250 V. The inner PEA was kept constant at 185 V and the amplitude of the a.c. voltage to study the elastocaloric effect was between 0.25 V and 0.5 V. **b**, A detailed view of the mounted sample and the shielded capacitor plates, indicated by the dashed black box. The applied strain was determined by measuring the displacement of a capacitor mounted in parallel to the sample. **c**, The configuration of the electronic setup for the ultra-low-noise measurement of the temperature oscillations. The solid yellow lines represent the thermocouple, the dotted red lines the twisted copper wires and the dotted black lines twisted NbTi wires. The thermocouple wires are soldered to twisted copper wires, which were thermally anchored on the thermometry stage. From there, twisted superconducting wires, to reduce the input impedance, are connected to the input of a shielded low-temperature transformer, which is thermally anchored on the 1-K pot of the dilution refrigerator. Finally, the voltage is measured at room temperature using a lock-in amplifier.

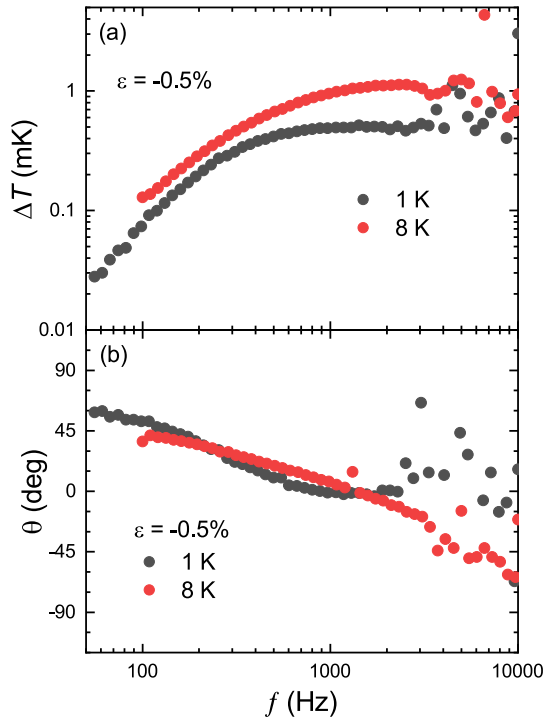

Extended Data Fig. 5 | Frequency response of the thermocouple. Elastocaloric effect under 0.5% compression at 1 K and 8 K plotted against a logarithmic frequency scale. The applied strain oscillation is $\Delta\varepsilon = 3.45 \times 10^{-6}$.

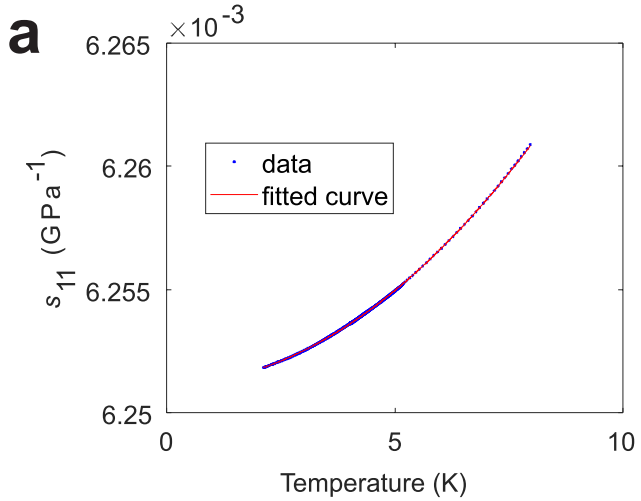

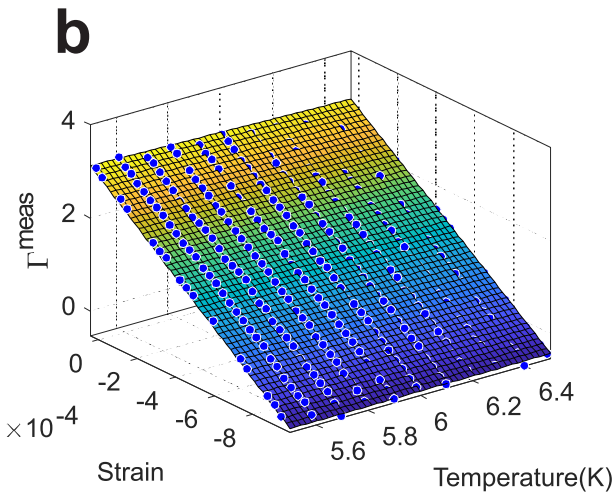

Extended Data Fig. 6 | Data from a resonant ultrasound experiment and result of the calibration procedure of the Grüneisen parameter. a, s_{11} as a function of temperature determined in independent resonant ultrasound measurements together with a fit of the form shown in Equation (15). **b**, Measured Grüneisen parameter compared with the calibration function. The spheres correspond to the data and the surface to Equation (16) with the parameters mentioned in the text.